ORIGINAL ARTICLE

lajss.org© Latin American Journal of Solids and Structures

www.lajss.org

Fault Diagnosis of Motor Bearing Based on Current Bi-Spectrum and Convolutional Neural Network

Jiaojiao Ma[a], Lingli Jiang[a], Shuhui Li[a], Heshan Sheng[a], Cheng Zhou[b], Xuejun Li[a]*

[a]School of Mechanical and Electrical Engineering, Foshan University, Foshan 528000, China. E-mail: majiaojiao@fosu.edu.cn, linlyjiang@163.com, 18872330348@163.com, 13213351140@163.com, hnkjdxlxj@163.com
[b]Chengdu CRRC Electric Motor Co. Ltd, Chengdu 610500, China. E-mail: 011600004656@crrcelectric.com

* Corresponding author

https://doi.org/10.1590/1679-78257364

Abstract

Motor bearings are prone to different degrees of performance degradation, fatigue damage and failure undergoing complex and harsh environments. Vibration signal analysis is a mature method for diagnosing motor bearing faults, while it is not applicable for installing additional vibration sensors on many occasions. Practically, the fault of motor bearings changes the air gap flux between the rotor and stator, which leads to harmonic fluctuations in the stator current. The current signals can be used to diagnose the motor bearing faults without additional sensors. Inevitably the harmonics caused by the motor bearing faults will be coupled with the original signals. This paper combines bi-spectrum and Convolution Neural Network (CNN) to analyze the current signals of motor bearing faults. The CNN diagnosis model is trained based on the local bi-spectrum of current, and the CNN parameters are optimized. Diagnose and analyze motor bearing faults with different fault implantation methods, working conditions, fault degrees and fault locations. The diagnostic accuracy reaches more than 80%.

Keywords

motor bearing; fault diagnosis; current; bi-spectrum; convolutional neural network

Graphical Abstract

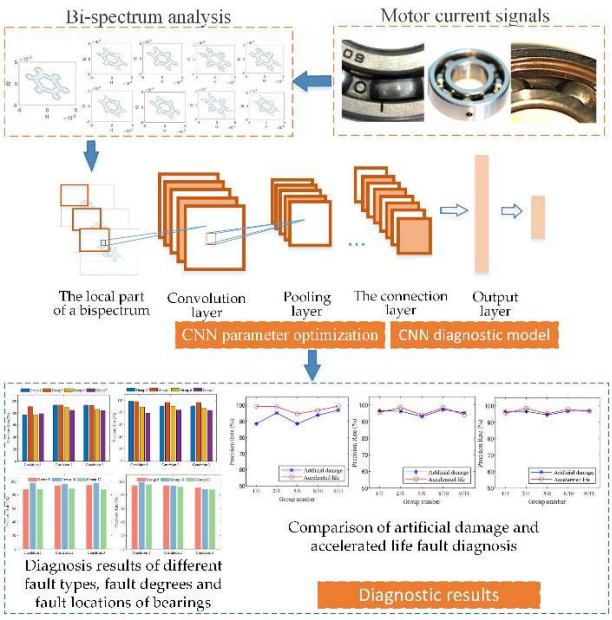

Received November 09, 2022. In revised form March 27, 2023. Accepted April 18, 2023. Available online April 24, 2023.
https://doi.org/10.1590/1679-78257364

Latin American Journal of Solids and Structures. ISSN 1679-7825. Copyright © 2023. This is an Open Access article distributed under the terms of the Creative Commons Attribution License, which permits unrestricted use, distribution, and reproduction in any medium, provided the original work is properly cited.

1 INTRODUCTION

Motor bearings are the crucial components of motors or engines, and their performance affects the property of industrial machinery. According to the statistics, motor failure is mainly caused by the faults of bearings. The ratios of bearing faults leading the motor broken in large machines and small machines are nearly 40 per cent and 90 per cent, respectively(Rifat, Pietro and C. 2018). Therefore, Effective monitoring and diagnosis of bearing conditions are significant for the operation of the motor. Vibration diagnosis method is the most mature and effective method at present (Adnani et al., 2016). It can diagnose common motor bearing faults and is widely used. However, the vibration diagnosis method requires new monitoring equipment such as sensors and signal acquisition units, and changes the original test interface of the motor. It is an invasive diagnostic method. For existing industrial motors, the project implementation is too difficult and cannot be applied on many occasions. The electrical diagnosis method comes into being(Gesseneck et al. 2016, Hamadache et al. 2015, Dhomad and Jaber 2020). The electrical method uses electrical data such as the speed, torque, and current signals of the motor drive to detect the bearing faults of the motor. It does not need to add additional sensors, which is a non-invasive fault diagnosis method. In the electrical method, it is common to use the motor stator current as the basis for fault diagnosis(Xiang et al. 2022, Hisahide and Yukio 2022). Bearing defects will lead to a specific air gap eccentricity and cause load torque oscillation, resulting in fluctuations in the stator current. In other words, the current signal contains bearing fault information. Safin et al. (2016) represented the characteristic harmonic component of stator current in an induction motor with faulty bearings during operation. Allal and Khechekhouche (2022) discovered performance in that the residual harmonic is often displayed at a fixed frequency when monitoring the rotor faults. Sun et al. (2020) used Hilbert-Huang Transform to extract fault features based on cavitation performance from current signals for cavitation detection in centrifugal pumps.

The above research is to extract the motor fault harmonic information from the current signal to achieve the purpose of diagnosis. Different types of faults have different harmonic characteristics. The influence of noise increases the difficulty of current fault feature extraction(Fu et al. 2023). In this regard, some researchers have used motor current combined with machine learning to diagnose motor faults. Wang et al. (2012) used different pattern classifiers to diagnose rotor faults from the motor current and current envelope signals. The results show that the diagnostic accuracy varies greatly with different combinations of features and pattern classifiers. Toma et al.(2020) extracted statistical features from motor current signals, and evaluate the bearing faults using genetic algorithms and three different classification algorithms. It can be seen that machine learning can well realize the current signal fault identification, and the selection of feature quantity and machine learning method will affect the diagnosis effect.

Signal bi-spectrum based on high-order statistics can be used to quantify the quadratic phase coupling between signal components and can suppress the influence of Gaussian colored noise and symmetric distribution noise, which is suitable for extracting signal feature information from the noise environment. Yang and Zhao (2012)proposed a fault feature extraction approach based on Empirica1 Mode Decomposition (EMD) and then analyzed the fault diagnosis of traction motor bearings based on the bi-spectrum characteristics of the vibration signals. Hassan et al. (2018) extracted features from the cross-bi-spectrum for the fault detection and diagnosis of a rotating mechanical system. Liang, Jiang and Qin (2020) found that the 1.5D spectrum features and bi-spectral features of signals were an advantage to realising the tooth surface wear of planetary gearboxes. The above methods are usually used to extract spectrum features from the bi-spectrum or further calculate other presentation parameters to diagnose the faults of crucial components. Bi-spectral image distribution itself can characterize the fault. Different kinds of faults, different degrees of faults, even under various working conditions, bi-spectrum has obvious differences, which can be directly used to characterize bearing faults.

Convolutional neural network(CNN) shows an excellent ability to feature autonomous learning and pattern recognition in the fields of object detection(Zhao and Li 2019, Wang et al. 2019, Fu et al. 2022) and image classification(Li et al. 2022, Zong et al. 2023). In recent years, the CNN technique has been widely used to identify and distinguish the multiple faults in the machinery field. The fault features were obtained directly from the original signal by CNN using its powerful feature autonomous learning ability. Chunzhi et al. (2018) used a one-dimensional convolution neural network to extract fault features from gearbox vibration signals and completed its diagnosis. Skowron(Skowron, Orlowska-Kowalska and Kowalski 2022) detected Permanent Magnet (PM) Faults Using a Convolutional Neural Network (CNN) Based on Original Stator Current Data. Huang et al. (2022) defined a novel dual-stream CNN that combined the classified by the linear weighting with the characteristics of signals in time domain and frequency domain. With the successful application of CNN in image recognition, it was also employed for the faults diagnosis depending on the transfer of the original time-domain signals into the 2D images and then used to train the classification models of CNN as the input parameter. Miao et al. (2019)used wavelet transform (CWT) to extract two-dimensional time-frequency maps from signals as input to CNN to classify and identify the defects of narrow lap weld. Tsai et al. (2022)proposed a

time-frequency analysis method of multi-sensor signal fusion to diagnose the Thruster Blade Fault. Chen et al. (2020) defined a new method depending on the deep learning technique, which combined Cyclic Spectral Coherence (CSCoh) with a 2D mapping representation of CNN. The accuracy of fault recognition is improved. According to the literature, it can be concluded that 2D images as the input parameters of CNN are effective and feasible to identify the mechanical faults.

This paper identifies the motor bearing faults based on the current signals. According to the advantage of CNN in image recognition, the bi-spectrum characteristics of signals are defined as the input samples of CNN and consequently classify and identify the motor bearing faults. Considering the symmetry of the bi-spectrum, there will be a lot of redundant information and leading to the reduction of CNN training efficiency, when the input sample is the bi-spectrum. Therefore, the local bi-spectrum is used to replace the global bi-spectrum to improve the training speed of CNN. The effects of the CNN application mainly depend on the designed architecture. The classification accuracy of CNN can be effectively improved by a reasonable selection of parameters, such as the layers' number, convolution kernels' number, convolution kernels' size and the step size of convolution kernels. In this paper, the local bi-spectrum of the motor bearing current is used to construct the input sample of CNN and the key architecture parameters of CNN can be optimized to improve the accuracy of motor bearing fault diagnosis.

2 Method of the current bi-spectrum CNN

2.1 Signal bi-spectrum extraction

The higher order moment, higher order cumulant, higher order moment spectrum and higher order cumulant spectrum are the main components of the higher order statistics method. Among them, the higher order cumulant and higher order cumulant spectrum are considered the crucial mathematical tools to analyze non-Gaussian random process(Xu et al. 2014), for the advantages of resisting the interference of Gaussian colored noise. The bi-spectrum is the most common one among high-order cumulant spectrum and is a third-order moment function which shows its effectiveness in quadratic phase coupling peak detection(Mendel JM. 1991).

Bi-spectrum can be calculated by the Fourier transform (FT) of third-order cumulant. The bi-spectrum has a lower order and complexity among the higher order spectra, but it is very practical. Considering the mean of the non-stationary random signal $x(n)$ is 0, and its autocorrelation function is expressed by

$$r(\tau) = E\{x(n)x(n+\tau)\} \tag{1}$$

where $E\{x(n)x(n+\tau)\}$ denotes mathematical expectation, τ means delayed time. The power spectrum is calculated based on the FT of the autocorrelation function.

$$p(w) = \sum_{-\infty}^{+\infty} r(\tau)\exp\{-j(\omega\tau)\} \tag{2}$$

The third-order cumulant descripts the statistical correlation between signal $x(n)$ and the other two delay forms $x(n+\tau_1)$, $x(n+\tau_2)$, and the caculated expression is

$$R(\tau_1,\tau_2) = \mathrm{cum}[\mathrm{x}(n), \mathrm{x}(n+\tau_1), \mathrm{x}(n+\tau_2)] \tag{3}$$

Then, bi-spectrum is defined by

$$B(\omega_1,\omega_2) = \sum_{\tau_1=-\infty}^{+\infty}\sum_{\tau_2=-\infty}^{+\infty} R(\tau_1,\tau_2)\times e^{-j(\omega_1\tau_1+\omega_2\tau_2)} \tag{4}$$

The bi-spectrum also can be expressed by the non-stationary random signal *x* in the frequency domain *X*(*ω*).

$$B(\omega_1,\omega_2)=X(\omega_1)X(\omega_2)*X(\omega_1+\omega_2) \tag{5}$$

where ω means the frequency.

According to the nature of the "semi-invariance" of higher order cumulant, the signal bi-spectrum can avoid Gaussian colored noise completely and consequently the details of signals, namely the minor components of signals can be extracted. Therefore, signal bi-spectrum can be used to quantify the quadratic phase coupling between signal components and suppress the influence of Gaussian colored noise and symmetric distribution noise, which is suitable for extracting signal feature information from the noise environment. For bi-spectrum of quadratic phase coupling harmonic processes, the peak values of signal bi-spectrum appear at the (ω_1,ω_2) and (ω_2,ω_1), and the value is zero at other frequencies. According to the bi-spectral image including the distribution and amplitude, the faults can be characterized, as shown in Figures 6-8. For the different kinds of faults and different degrees of faults, even under various working conditions, the bi-spectrum will be different.

2.2 CNN and its parameter optimization

The main components of CNN structure include the convolutional layer, the pooling layer and the fully connected layer. Among them, the convolution layer can be used to extract features from the input images' information, the pooling layer compresses the extracted features, and the fully connected layer completes the final classification task. The relationship between them is demonstrated in Figure 1. The local part of a bispectrum of current signals as the input is used to optimize the structure of the CNN by trial and error.

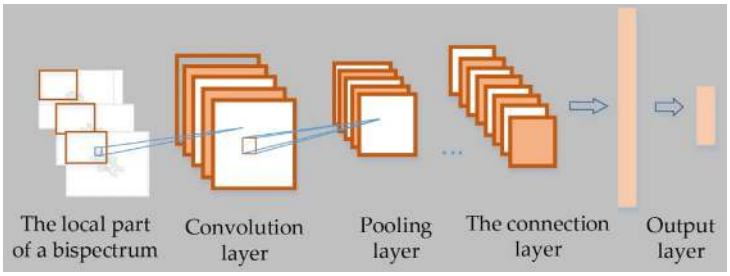

Figure 1: CNN framework.

The architecture of CNN determines its performance, the main influencing parameters are introduced and the effects of parameter settings are analyzed as follows.

The number of convolutional layers: The number of convolutional layers determines the depth of the network, which also determines the complexity of the network. Within a certain range, the more layers, the more nonlinear expression ability of the network, the clearer the extracted features, and the better the effect of pattern recognition. However, a deep network leads to more complex models and reduced training efficiency.

The number of convolution kernels: The features of the signals can be extracted by the convolution kernels. It can be beneficial to the feature maps and the model fitting ability with a larger number of convolution kernels, but too many convolution kernels will easily lead to overfitting.

Convolution kernel size: the parameters and computation will be reduced as the convolution kernel is set as a small value in the case of reaching the same receptive field.

Convolution kernel step size: The convolution kernel slides on the data with a certain step size, and in order to avoid loss of information, the step size is set smaller than that of the convolution kernel. Simultaneously, a smaller step size will result in more sufficient scanned data, and it is easier to obtain complete feature information. However, the more noise information that is repeated at the same time will reduce the generalization ability of the model.

Batch size: refers to the sample size used for parameter learning. Using large batch sizes during training may reduce the randomness of network gradient descent. Using smaller batch sizes results in more volatile and random weight updates, which can help training jump out of local minima.

Learning rate: Learning rate can have a huge impact on the difficulty of network training. Practically, the learning rate is usually inversely proportional to the convergence rate of the network.

Epoch number: refers to the number of times the whole training set is input to CNN for training. When the network accuracy is on the rise, the number of iterations should be increased.

Based on the above analysis, the ability and recognition accuracy of CNN to extract the fault information of motor bearings can be improved by reasonable optimization of the above parameters.

2.3 Description of current bi-spectrum CNN

According to the symmetry, some quadrants of the bi-spectrum are intercepted in this paper and used as input data of CNN for diagnosis and analysis of motor bearings. The local image captured in this paper is a 1/4 bi-spectral image, which contains the fault global information and removes the redundant information, and then it is employed for model training and testing. Figure 2 describes the diagnosis of motor bearing faults using the method under the combination of local bi-spectrum and CNN. The detailed process is as follows:

1. Bi-spectrum analysis is performed based on the selected current signal data, which is set to obtain bi-spectrum.
2. The 1/4 image that can represent the global information of the bi-spectrum is captured to obtain the local bi-spectrum.
3. The structure of CNN is designed depending on the parameter optimization sample library and the data is divided into a sample set, test set and validation set. The parameters of the CNN are optimized in combination with the guaranteed recognition accuracy.
4. The local bi-spectral map is used as the input to derive the CNN model of the motor bearing diagnosis based on the optimized parameters.
5. The local bi-spectrum of the sample to be diagnosed is input and the diagnosis result is obtained.

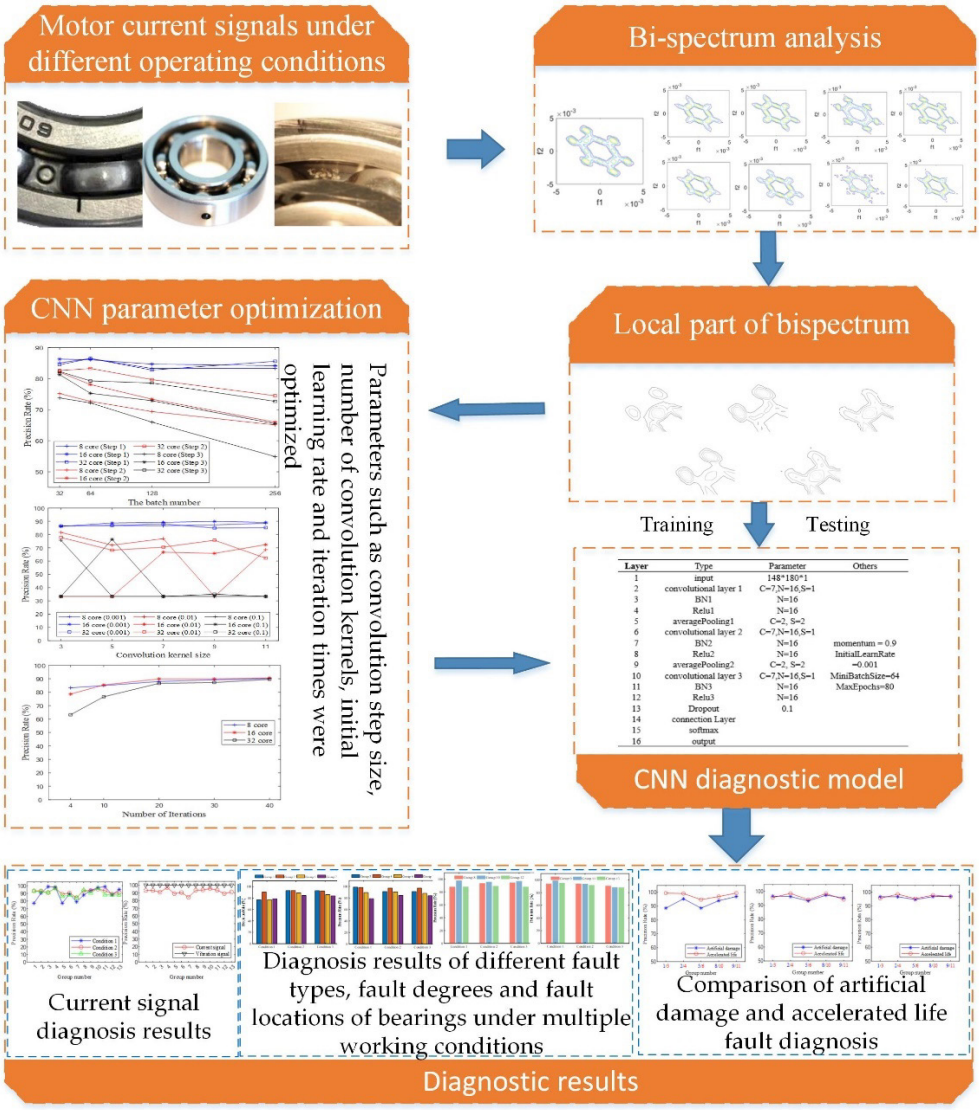

Figure 2. Diagnosis process.

3 EXAMPLES OF MOTOR BEARING FAULT DIAGNOSIS

3.1 Data acquisition

The case analysis data is derived from the University of Paderborn Bearing dataset, which was published by Christian Lessmeier et al in 2016. The test bench is set up as shown in Figure. 3, which is mainly composed of five main components, including (1) driving motor, (2) torque measuring shaft, (3) bearing test module, (4) flywheel and (5) load motor from left to right.

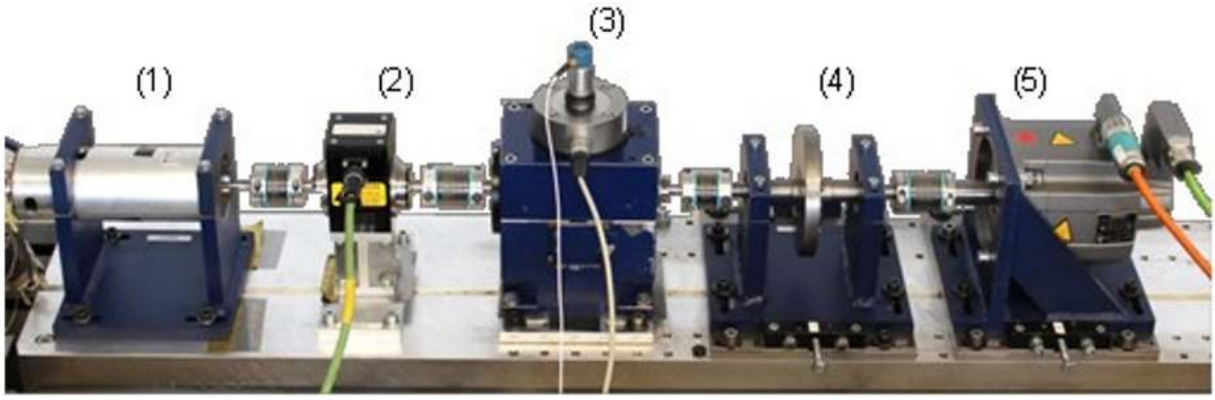

Figure 3. Test rig.

The bearing test module can replace the test bearings with different fault modes according to the test requirements, and a constant radial load can be applied to the test bearings during the test, which can be adjusted within (0~10 KN). The flywheel and load motor simulate the inertia and torque of the test bearing respectively.

During the test, a current sensor was used to replace the internal ammeter of the inverter. The model of the current sensor was LEM CKSR 15-NP, and the accuracy of the sensor could reach 0.8% IPN (IPN is the full-scale value, IPN=15 A). Selecting the frequency band should cover the fault information that can better identify the fault accurately, and the fault information of bearings is mainly reflected in the low frequency range (below a few tens of kHz). The frequency bands are selected conventionally. The data used to analyze is derived from the University of Paderborn Bearing dataset, where a low-pass filter of 25 kHz was set at the sampling front for the current signals and a low-pass filter of 30 kHz was set for the collected vibration signals. Based on the Nyquist-Shannon sampling theorem, the sampling frequency here is set as 64 kHz. The vibration signal was collected synchronously during the test to facilitate the comparison and analysis with the current signal. PCB integrated acceleration sensor is adopted, and the sensor is installed on the bearing seat. The sampling front end is set with a low-pass filter of 30 kHz, and the sampling frequency is 64 kHz. To record the operating conditions, the radial force, load torque, speed and oil temperature of the test bearing are measured synchronously with the current and vibration signals at a lower sampling frequency.

Test-bearing fault parts include manual implantation faults, as shown in Figure 4; As shown in Figure 5, failure occurred during fatigue life test operation. The bearing data under different working conditions are obtained by changing the motor speed, load torque of the load motor and radial force on the test bearing. The three working conditions are shown in Table 1. The operation data under three working conditions, different fault implantation methods, different fault types and different fault degrees collected by the test are taken, and the corresponding data description is shown in Table 2.



Figure 4. Artificially damaged bearings.

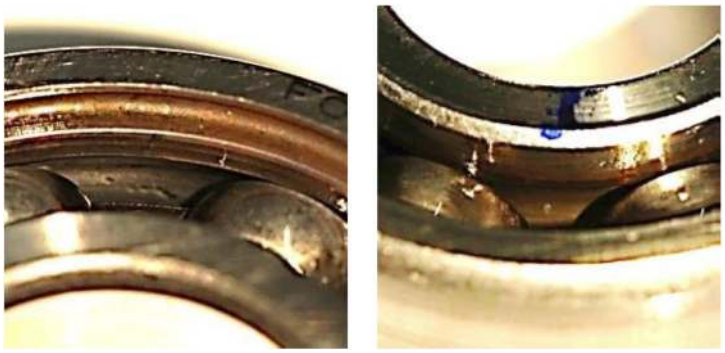

Figure 5. Faults of bearing running on fatigue accelerated life testing machine.

Table 1. Description of three working conditions.

Working Condition	Rotate Speed [r/min]	Load Torque [Nm]	Radial Force [N]	Set Name
1	900	0.7	1000	N09_M07_F10
2	1500	0.7	400	N15_M07_F04
3	1500	0.7	1000	N15_M07_F10

Table 2. Data specification.

Serial Number	Data	State	Degree of fault	Type
1	K005	Normal	--	----
2	KA05	Outer ring fault	1	Manual implantation fault
3	KA03	Outer ring fault	2	Manual implantation fault
4	KA04	Outer ring fault	1	Accelerated life test fault
5	KA16	Outer ring fault	2	Accelerated life test fault
6	KI03	Inner ring fault	1	Manual implantation fault
7	KI07	Inner ring fault	2	Manual implantation fault
8	KI21	Inner ring fault	1	Accelerated life test fault
9	KI18	Inner ring fault	2	Accelerated life test fault

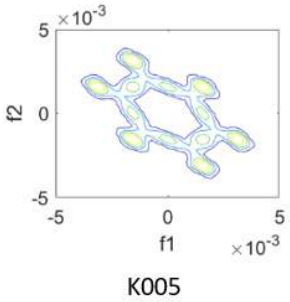

Figure 6. Bi-spectrum of current in normal states.

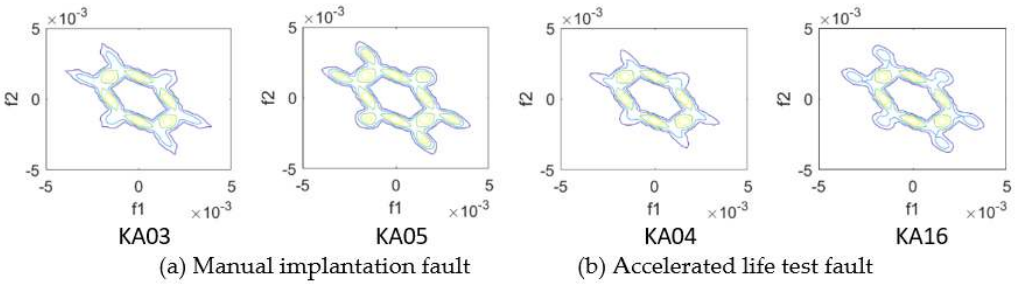

Figure 7. Bi-spectrum of current in outer ring failure states.

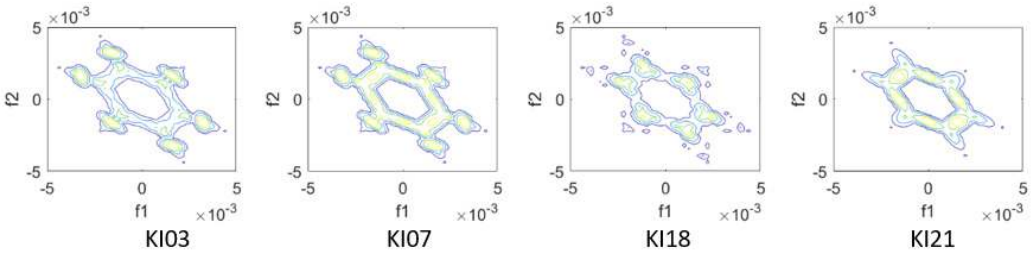

Figure 8. Bi-spectrum of current in inner ring failure states.

3.2 Bi-spectrum analysis

The bi-spectrum of motor bearing current in different fault states under representative working conditions (working condition 3: input speed 1500RPM, torque 0.7N.m, radial load 1000N) were compared and analyzed. The current bi-spectrum under normal conditions is analyzed in Figure 6, the results of the current bi-spectrum when the outer ring is faulty are represented by Figure 7, and Figure 8 shows the current bi-spectrum when the inner ring is faulty. As can be seen from Figures 6-8, for bearing faults in the same position (such as inner ring faults), the morphology of the bi-spectrum is similar whether the fault is artificially implanted in different forms or the fault in different forms produced by the fatigue accelerated life testing machine. There are differences in the bi-spectrum of bearing normal state, inner ring fault and outer ring fault. Therefore, the current bi-spectrum has the ability to characterize bearing fault types.

3.3 CNN parameter optimization

The samples of three operating conditions are used to construct the sample set for CNN parameter optimization (normal state K005, outer ring fault KA03, inner ring fault KI07) under representative working conditions of speed 1500 RPM, torque 0.7 N.m and radial load 1000 N (working condition 3). For the convenience of computing, the activation layer of CNN adopts a linear rectification function, which improves the training speed and avoids overfitting. The initial value of the learning rate is set as 0.001, the number of convolution kernels is 16, and the size of convolution kernels is 3*3. Meanwhile, step sizes of convolution kernels are different and set as 1, 2 and 3 respectively. The number of different convolution kernels is 8, 16 and 32, respectively.

The accuracy of fault identification under different batch sizes is compared, and the test results are shown in Figure 9. In the figure, with the increase in batch number, the overall accuracy presents a downward trend. Furthermore, as the number of convolution kernels decreases, the accuracy will also decrease. When the convolution kernel step is 1, it has a better recognition effect.

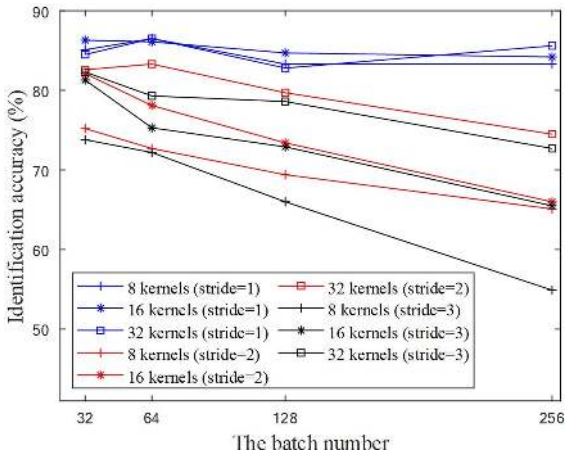

Figure 9. Accuracy rate under different convolution steps and the number of convolution kernels.

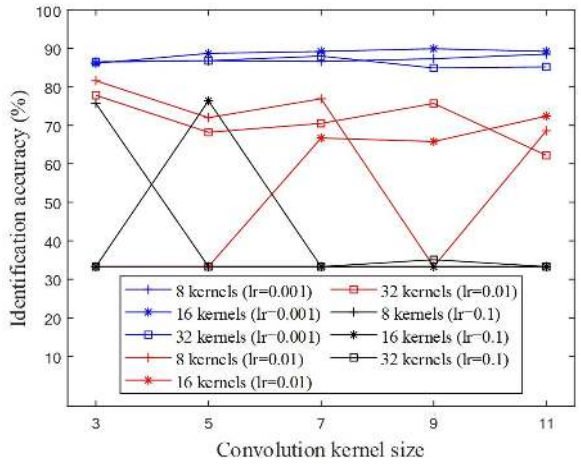

Figure 10. Accuracy rate under different convolution kernel sizes and different initial learning rates.

Combined with the above analysis results, when the convolution kernel step size is selected as 1, the accuracy of fault identification is discussed under different initial learning rates and different convolution kernel sizes. The results are shown in Figure 10. When the initial learning rate is set by 0.001, the accuracy has a relatively stable trend and does not change dramatically with the change in the convolution kernel size.

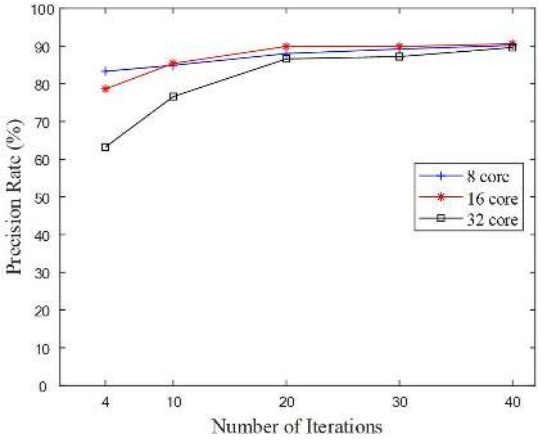

Figure 11. Accuracy rate under different epochs.

In addition, the effect of iteration number on accuracy is further analyzed. The values of iteration times are set to include 4, 10, 20, 30 and 40. Figure 11 demonstrates the test results. The accuracy increases as the number of iterations increases. However, as we all know, the number of iterations will affect the recognition time, so it should not be selected too large.

3.4 Results Analysis

The parameters, including the iterations of CNN, the number of convolution kernels and steps, the size of convolution kernels and the initial learning rate are obtained by comparison optimization. The 'sgdm' (driven stochastic gradient descent) optimizer is used to construct the CNN diagnostic model. The CNN model parameters are summarized in Table 3, where C denotes the size of the convolution kernel, N is the number of convolution kernels, and S means the step size of convolution.

To discuss the diagnostic accuracy of different working conditions, fault implantation methods, fault degrees and fault locations, and to compare with the vibration diagnosis method, are further grouped based on the experimental data in this paper, as shown in Table 4. The corresponding diagnostic results can be seen in Table 5.

Table 3. CNN model parameters.

Layer	Types	Parameter	Other Parameter
1	Input layer	148*180*1	
2	Convolution layer 1	C=7,N=16,S=1	
3	BN1	N=16	
4	Relu1	N=16	
5	averagePooling1	C=2, S=2	
6	Convolution layer 2	C=7,N=16,S=1	
7	BN2	N=16	momentum = 0.9
8	Relu2	N=16	InitialLearnRate
9	averagePooling2	C=2, S=2	0.001
10	Convolution layer 3	C=7,N=16,S=1	MiniBatchSize=64
11	BN3	N=16	MaxEpochs=80
12	Relu3	N=16	
13	Dropout	0.1	
14	Connection layer		
15	softmax		
16	output layer		

Table 4. Group of Experiments.

	Group number	Dataset		
		Normal	Outer ring fault	Inner ring fault
Fault Type Classification	1	K005	KA05	KI03
	2	K005	KA03	KI07
	3	K005	KA04	KI21
	4	K005	KA16	KI18
	5	K005	KA05	KI03
			KA03	KI07
	6	K005	KA04、KA16	KI21、KI18
	7	K005	KA05、KA03	KI03、KI07
			KA04、KA16	KI21、KI18
	Group number	**Normal**	**Minor fault**	**Severe faults**
Fault degree classification	8	K005	KA05	KA03
	9	K005	KI03	KI07
	10	K005	KA04	KA16
	11	K005	KI21	KI18
	12	K005	KA05、KA04	KA03、KA16
	13	K005	KI03、KI21	KI07、KI18

Figure 12 shows the diagnosis results of 13 sets of data of current signals under three different working conditions: working condition 1 (900 RPM, 0.7 Nm, 1000 N), working condition 2 (1500 RPM, 0.7 Nm, 400 N) and working condition 3 (1500 RPM, 0.7 Nm, 1000N). The diagnostic rates of the three groups of data in working condition 1 are slightly lower than 80%, the diagnostic rates of the other groups of data are all above 80%, and the accuracy rates in working conditions 2 and 3 are around 90%. The speed of 900 RPM is defined as working condition 1, and working conditions 2 and 3 have the same speed of 1500 RPM. It can be seen that speed has a great influence on fault occurrence, and the greater the speed, the more obvious the fault occurrence. Conditions 2 and 3 are both 1500 RPM, but the radial load is different. The diagnosis results of conditions 2 and 3 are similar under different grouping conditions, so it shows that the radial load has little influence on the appearance of the fault.

Table 5. Diagnostic results.

Group number	Condition 1		Condition 2		Condition 3	
	Current	Vibration	Current	Vibration	Current	Vibration
1	77.1%	100%	93.2%	100%	93.1%	100%
2	90.5%	99.4%	93.2%	100%	92.4%	100%
3	98.8%	100%	91.0%	100%	91.1%	100%
4	98.2%	100%	96.9%	100%	96.9%	100%
5	77.1%	100%	89.1%	100%	86.1%	100%
6	89.3%	100%	90.5%	100%	87.9%	99.8%
7	78.9%	100%	84.4%	99.9%	83.9%	99.7%
8	87.8%	100%	93.4%	100%	94.4%	100%
9	93.8%	99.4%	93.8%	100%	90.5%	100%
10	97.6%	100%	95.5%	100%	96.7%	100%
11	98.8%	100%	93.6%	100%	88.2%	100%
12	88.1%	100%	89.1%	99.9%	87.9%	99.9%
13	95.1%	100%	91.2%	99.9%	87.9%	100%

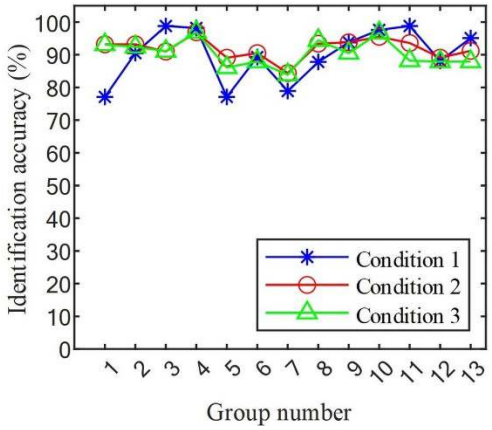

Figure 12. Diagnostic result test under different conditions.

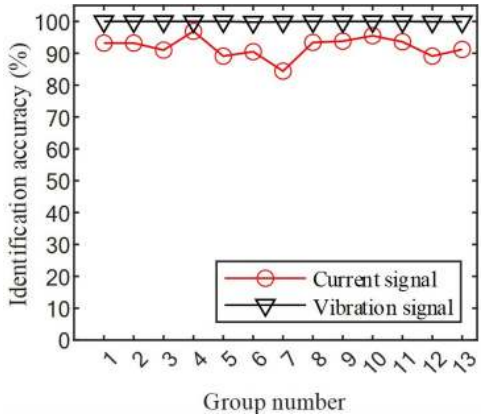

Figure 13. Comparison of diagnostic results of vibration signal and current signal.

Figure 13 shows the diagnosis of the current signal and vibration signal under working condition 2. Comparing the results, the accuracy of vibration signals is higher than that of current signals, but the accuracy difference is less than 10%. Considering portability and applicability, the fault diagnosis method based on current is reliable for motor bearing fault diagnosis and shows an advantage.

The current signal diagnosis of artificial implantation injury and accelerated life test faults are studied and the results show in Figure 14. Working at condition 1, the diagnostic rate of artificial implantation injury is lower than that of test implantation injury. Working at conditions 2 and 3, the diagnostic accuracy of the two fault implantation methods is similar. The results show that the method can be used to diagnose the faults not only caused by the accelerated life but

also the artificial fault implantation adopted. Therefore, it is feasible to acquire research data by artificial implantation of faults under limited or hard conditions to obtain the actual fault information directly.

Figure 15 describes the results caused by different types of bearing faults. It is clear that fault-type diagnosis accuracy increases the deepening of the fault degrees. In addition, the different fault types can be accurately identified by the method even if the different degrees of faults are mixed.

Figure 16 shows the comparison of fault degree diagnosis results under single fault implanted samples and mixed fault implanted samples in the current diagnosis method. It can also be found that different fault degrees can be accurately identified even if different samples are mixed.

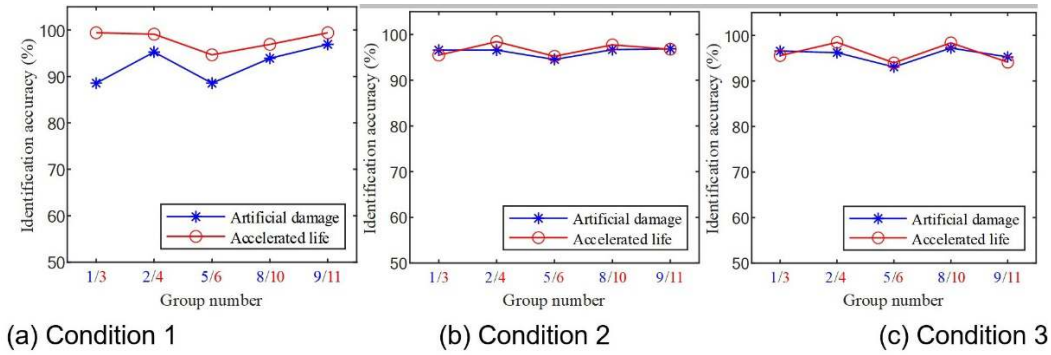

Figure 14. Comparison of implant fault diagnosis result between artificial implant fault and accelerated life test.

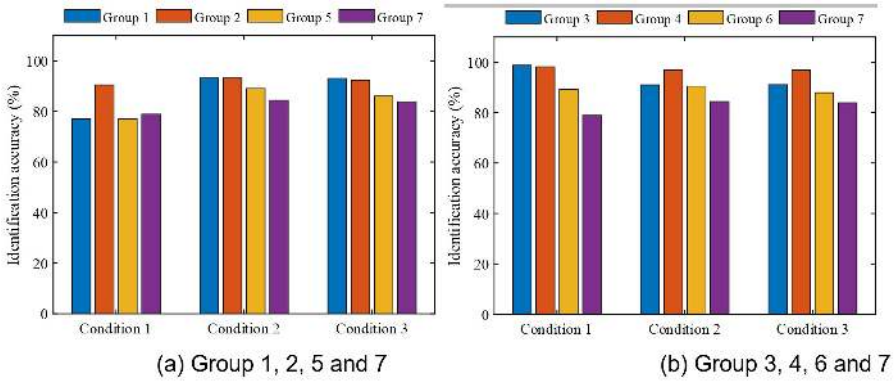

Figure 15. Comparison of diagnostic results of different fault types.

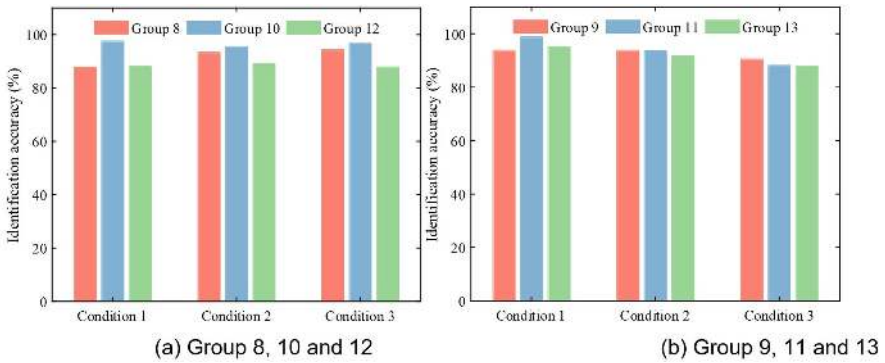

Figure 16. Comparison of diagnostic results of different fault locations.

4 CONCLUSIONS AND PROSPECT

Aiming at the difficulty of collecting vibration signals of motor bearings in industrial applications, a fault diagnosis method of motor bearings based on easily obtained current signals was developed. The method of current bi-spectral CNN was proposed. By grouping and analyzing the data under various working conditions, fault implantation methods, kinds of faults and fault degrees, the following conclusions are drawn:

(1) The method of current bi-spectral CNN is effective to identify the faults of motor bearings. Although the diagnostic accuracy is not as high as that of vibration bi-spectral CNN, it has greater application and promotion prospects because the current signal is easier to obtain.
(2) Under different speed and load conditions, the effect of the same bearing fault represented in the current signal is different. Speed has a great influence on the fault. The greater the speed, the more obvious the fault is.
(3) The artificial fault implantation adopted is comparable to the fault diagnosis result obtained by the fatigue life test, and it is feasible to obtain the research data by artificial fault implantation.
(4) Different fault types can still be accurately identified by mixing samples of different fault degrees; By mixing samples of different fault implantation methods, different fault degrees can still be accurately identified. The validity of the current bi-spectrum CNN motor bearing fault diagnosis method is further illustrated.

The current signal is easy to obtain. Therefore, the current bi-spectral CNN will have a wider application. For motor bearings, due to the variable working conditions and overlapping fault modes of each component in practical application, there may be multiple modes of secondary phase coupling in current signals, which makes the analytical analysis of the bi-spectrum more difficult. In the future, signal processing methods for current signals can be further studied to improve diagnostic accuracy.

Acknowledgement

This work was supported by the National Key Research and Development Program (Grant Nos. 2020YFB2007805), the Guangdong Basic and Applied Basic Research Foundation (Grant Nos. 2021A1515110767) and the Scientific Research Project of Guangdong Provincial Department of Education (Grant Nos. 2022ZDZX3025).

Author's Contributions: Conceptualization, J.M. and L.J.; methodology, J.M. and X.L.; software, S.L. and H.S.; validation, X.L. and L.J.; formal analysis, J.M. and H.S.; investigation, J.M. and X.L.; resources, J.M. and C.Z.; data curation, L.J.; writing—original draft preparation, S.L. and L.J.; writing—review and editing J.M.; visualization, L.J. and C.Z.; supervision, J.M.; project administration, X.L. All authors have read and agreed to the published version of the manuscript.

Editor: Pablo Andrés Muñoz Rojas

References

Rifat, S. M., B. Pietro and T. A. C. C., (2018). Electrical Signature Analysis-Based Detection of External Bearing Faults in Electromechanical Drivetrains. IEEE Transactions on Industrial Electronics, 65: 5941-5950.

Adnani A A T, Dokami A, Morovati M., (2016). Fault Detection in High Speed Helical Gears Considering Signal Processing Method in Real Simulation[J]. Latin American Journal of Solids and Structures, 13: 2113-2140.

Gesseneck, J. J. v., B. Caers, M. V. Overmeire, D. Lefeber, B. Vanderborght and P. Schuurmans, (2016) A torque-based method for the study of roller bearing degradation under poor lubrication conditions in a lead–bismuth environment. Nuclear Engineering and Design, 121-131.

Hamadache, Moussa, Lee, Dongik, Veluvolu and K. C., (2015). Rotor Speed-Based Bearing Fault Diagnosis (RSB-BFD) Under Variable Speed and Constant Load. IEEE Transactions on Industrial Electronics, 62: 6486-6495.

Dhomad, T. A. and A. A. Jaber, (2020). Bearing Fault Diagnosis Using Motor Current Signature Analysis and the Artificial Neural Network. International Journal on Advanced Science, Engineering and Information Technology, 10.

Xiang, L., Z. Ao, S. Yaqi, M. Guoli, B. Xingzhen and G. Yinjing, (2022). Application of Improved Robust Local Mean Decomposition and Multiple Disturbance Multi-Verse Optimizer-Based MCKD in the Diagnosis of Multiple Rolling Element Bearing Faults. Machines, 10:883.

Hisahide, N. and M. Yukio, (2022). Diagnosis for Slight Bearing Fault in Induction Motor Based on Combination of Selective Features and Machine Learning. Energies, 15:453.

Safin, N., V. Prakht, V. Dmitrievskii and A. Dmitrievskii, (2016). Stator current fault diagnosis of induction motor bearings based on the fast Fourier transform. Russian Electrical Engineering, 87: 661-665.

Allal, A. and A. Khechekhouche, (2022). Diagnosis of induction motor faults using the motor current normalized residual harmonic analysis method. International Journal of Electrical Power and Energy Systems, 141:108219.

Sun, H., Q. Si, N. Chen and S. Yuan, (2020). HHT-based feature extraction of pump operation instability under cavitation conditions through motor current signal analysis. Mechanical Systems and Signal Processing, 139:106613.

Fu, C., J.-J. Sinou, Zhu, W., Lu, K. and Y. Yang, (2023). A state-of-the-art review on uncertainty analysis of rotor systems. Mechanical Systems and Signal Processing, 183:109619.

Wang, J., S. Liu, R. X. Gao and R. Yan, (2012). Current envelope analysis for defect identification and diagnosis in induction motors. Journal of Manufacturing Systems, 31:380-387.

Toma, R. N., A. E. Prosvirin and J.-M. Kim, (2020). Bearing fault diagnosis of induction motors using a genetic algorithm and machine learning classifiers. Sensors, 20:1884.

Yang, J. and M. Zhao, (2012). Fault diagnosis of traction motor bearings using modified bispectrum and empirical mode decomposition. In Zhongguo Dianji Gongcheng Xuebao (Proceedings of the Chinese Society of Electrical Engineering). Chinese Society for Electrical Engineering; pp. 116-122.

Hassan, M. A., M. R. Habib, R. A. Abul Seoud and A. M. Bayoumi, (2018). Wavelet-based multiresolution bispectral analysis for detection and classification of helicopter drive-shaft problems. Journal of Dynamic Systems, Measurement, and Control, 140: 061009.

Liang, H., Z. Jiang and H. Qin, (2020). Fault diagnosis method of planetary gear box based on bispectral characteristics. Modular Mach. Tools Autom. Manuf. Tech., 110-113.

Zhao, D. and H. Li., (2019). Forward vehicle detection based on deep convolution neural network. In AIP Conference Proceedings, AIP Publishing LLC; 020107

Wang, J., T. Zheng, P. Lei and X. Bai, (2019). A hierarchical convolution neural network, (CNN)-based ship target detection method in spaceborne SAR imagery. Remote Sensing, 11:620.

Fu, C., W. Zhu, Z. Zheng, C. Sun, Y. Yang and K. Lu, (2022). Nonlinear responses of a dual-rotor system with rub-impact fault subject to interval uncertain parameters. Mechanical Systems and Signal Processing, 170:108827.

Li, T., Y. Yin, Z. Yi, Z. Guo, Z. Guo and S. Chen, (2022). Evaluation of a convolutional neural network to identify scaphoid fractures on radiographs. Journal of Hand Surgery (European Volume), 17531934221127092.

Zong, S., G. Zhou, M. Li and X. Wang, (2023). Deep learning-based on-line image analysis for continuous industrial crystallization processes. Particuology, 74:173-183.

Chunzhi, W. U., P. Jiang, F. Feng, T. Chen and X. Chen, (2018). Faults diagnosis method for gearboxes based on a 1-D convolutional neural network. Journal of Vibration and Shock.

Skowron, M., T. Orlowska-Kowalska and C. T. Kowalski, (2022). Detection of permanent magnet damage of PMSM drive based on direct analysis of the stator phase currents using convolutional neural network. IEEE Transactions on Industrial Electronics.

Huang, E., X. Zheng, Y. Fang and Z. Zhang, (2022). Classification of Motor Imagery EEG Based on Time-Domain and Frequency-Domain Dual-Stream Convolutional Neural Network. IRBM, 43:107-113.

Miao, R., Y. Gao, L. Ge, Z. Jiang and J. Zhang, (2019). Online defect recognition of narrow overlap weld based on two-stage recognition model combining continuous wavelet transform and convolutional neural network. Computers in Industry, 112: 103115.

Tsai, C.-M., C.-S. Wang, Y.-J. Chung, Y.-D. Sun and J.-W. Perng, (2022). Multi-Sensor Fusion Time-Frequency Analysis of Thruster Blade Fault Diagnosis Based on Deep Learning. IEEE Sensors Journal.

Chen, Z., A. Mauricio, W. Li and K. Gryllias, (2020). A deep learning method for bearing fault diagnosis based on cyclic spectral coherence and convolutional neural networks. Mechanical Systems and Signal Processing, 140:106683.

Lessmeier, C., J. K. Kimotho, D. Zimmer and W. Sextro., (2016). Condition monitoring of bearing damage in electromechanical drive systems by using motor current signals of electric motors: A benchmark data set for data-driven classification. In PHM Society European Conference.

Mendel JM, (1991). Tutorial on higher order statistics (spectra) in signal processing and system theory: theoretical results and some applications. In: Proceedings of the IEEE, 79: 287-05.

Xu, X., Jiang, Z., Wang, H., Wu, G., Zuo, Y., Chen, P., Wang, L., (2014). Application of the state deterioration evolution based on bi-spectrum in wind turbine. Proceedings of the Institution of Mechanical Engineers, Part C: Journal of Mechanical Engineering Science, 228(11), 1958–1967.